JOURNAL OF GUIDANCE, CONTROL, AND DYNAMICS
Vol. 19, No. 1, January–February 1996

Global Structure Modeling Using Force-State Component Identification

Brett P. Masters* and Edward F. Crawley†
Massachusetts Institute of Technology, Cambridge, Massachusetts 02139
and
Marthinus C. van Schoor‡
University of Pretoria, Pretoria, South Africa

The nonlinear-dissipative modal behavior of a structure is predicted from measured component characteristics and compared with modal test data. The force-state component identification methodology is applied to multi-axis testing of deployable, erectable, and rotary joint components of the middeck 0-gravity dynamics experiment structure. Analytic models are are used to approximate the force-state data and are assembled into a global model. A linearization algorithm is used to predict frequency response of the model. Predictions correlate well with 0-gravity and ground test modal data that are shown to depend on joint preload, force amplitude, and gravity conditions. Moderately nonlinear behavior is both predicted and observed in the configuration containing the rotary joint.

Introduction

STRINGENT performance requirements on modern spacecraft create demands for increasingly accurate structural dynamic models. These demands imply that not only accurate linear models be constructed but also nonlinear and dissipative elements be included. Success of future missions, especially those incorporating active structural control, will depend on the ability of engineers to establish such models.

Typically, the evolution of a structural model has three stages. During development, a first generation dynamic model is derived from drawings and handbook data. Although this model can be used in performance studies, its accuracy is limited by initial assumptions and mismodeling errors.

A second generation model is normally obtained by updating this first model using measurements made on individual structural components. Common measurements, such as component weight and stiffness tests, are used to update component models. A third generation model is obtained by using data from dynamic testing on the assembled structure to update the second generation model.[1] Third generation models are not always obtainable prior to flight, since full vehicle dynamic ground testing may not be possible. When conducted, ground vibration tests often yield data corrupted by gravity and suspension effects.

In most instances, first and second generation models are linear or linearized, and seldom do they include nonlinearities and dissipation. The effects of stiffness nonlinearities induced by large amplitude motion, predeflections, and preloads in beams and plates have been studied extensively.[2,3] Limited work has been done, however, to combine joint nonlinearities with linear structural models to yield a coupled linear–nonlinear model for the purpose of dynamic response prediction.[4,5]

The research at Massachusetts Institute of Technology (MIT) on the inclusion of nonlinear effects in modal models is part of the middeck 0-gravity dynamics experiment (MODE). Open-loop dynamics testing of the structural test article was performed both on orbit (on STS-48) and in the ground-based laboratory. The STA is an engineering scale model that incorporates mainly two elements, each consisting of four wire-braced deployable bays. These deployable bays can be assembled into different configurations using the other elements in the STA hardware set. Figure 1 shows how the bays can be joined by a central erectable bay to form the baseline configuration or by an adjustable break load rotary (alpha) joint to form the alpha configuration.

The MODE dynamic test results exhibited forcing amplitude-dependent nonlinear frequency response characteristics.[6] This nonlinear behavior was observed in both the one- and zero-gravity test results. (For example, the upper graph of Fig. 7 shows that the nonlinearities cause softening and dampening of the structural modes with increased force.)

Force-state component identification[7] is one approach that can be used to generate second generation models of structures with nonlinear and dissipative elements. The objective of this work is to assemble a global structural model from nonlinear dissipative component models that have been experimentally identified and to verify the accuracy of that model by comparison with modal test data.

The multiple degree-of-freedom (DOF) force-state component identification methodology is presented first. The methodology is demonstrated by applying it to the MODE STA deployable, erectable, and alpha joint bays to yield analytical component models. Component models are obtained by fitting analytical functions to the force-state component data. The paper proceeds by discussing the component models and the inherent nonlinear mechanisms that drive their nonlinear and dissipative behavior.

The analytical models of the bays are then used to formulate global structure dynamic models of the two assembled configurations shown in Fig. 1. The global structure models are used to predict the nonlinear discrete frequency responses. These responses are obtained using a linearization algorithm that iterates on the least squares linear response at each discrete frequency point. The predictions are compared with modal test data for differing levels of excitation force, deployable bay pretension, alpha joint preload, and change in gravity environment.

Force-State Component Identification Methodology

The methodology for modeling nonlinear components of structural systems, such as the MODE STA, is incorporated in multiple

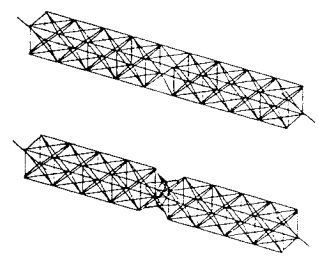

Fig. 1 Two test configurations of the STA, baseline (top) and alpha (bottom).

Received May 27, 1994; revision received May 28, 1995; accepted for publication July 31, 1995.

*Graduate Research Assistant, Space Engineering Research Center, 37-395 MIT. Student Member AIAA.
†Professor of Aeronautics and Astronautics, Space Engineering Research Center, 37-341 MIT. Associate Fellow AIAA.
‡Professor, Department of Mechanical Engineering and Aeronautics.

DOF force-state component identification.[7,8] This section introduces the general methodology of force-state mapping before describing the specialized approach used for the MODE components. The specialized approach includes the protocol for applying dynamic loads to the component and the identification algorithms used to identify the nonlinear constitutive models from component test data.

Traditionally, the modeling of local nonlinearities (such as joints) had been approached using load-stroke test information. Transmitted force that depends explicitly on velocity, coupled DOF, or on true memory effects can only be incompletely inferred from static force-displacement measurements. This deficiency was addressed by the development of multiple DOF quasistatic force-state component identification. In multiple DOF force-state component identification, the generalized forces transmitted through the component are represented as functions of the generalized displacements and velocities across the component.

Experimentally, the force-state component identification approach requires the application of dynamic loads to the component while measuring or estimating generalized forces, accelerations, displacements and velocities. The measured forces are corrected for the inertia force and coupled DOF structural forces before being conceptually plotted vs relevant displacement and velocity states of the component. Modeling proceeds by investigating the multiple force-state maps and deciphering the constitutive relations and mechanisms of the component.

The approach taken in previous work[7] was to characterize an entire bay of the truss structure undergoing shear, bending, extension, and twisting by treating the bay as a 12-DOF generally nonlinear beam element. One end of the bay was constrained while the unconstrained end was exercised in all 6 DOF (defined about the elastic centroid) in a test rig, as described in previous papers.[7,8]

Dynamic loads applied to a component mounted in the test rig are prescribed in terms of protocols for load directions and load time history. Two protocols of six applied load directions can be used: load-control for a set of six approximately decoupled generalized applied loads; and stroke-control for a set of six applied loads that approximately decouple the generalized 6-DOF response. Load control can be used for either stiff or soft components but is preferred over stroke control for soft, strongly nonlinear components, such as those incorporating an articulating mechanism. Load control is preferred in these components in order to avoid dynamic preloads that are on the order of the structural forces generated within the component. Stroke control is suggested for stiff, predominantly linear, components as this choice of inputs simplifies the ensuing identification algorithm. The loads time history used is a sinusoid ramped from zero amplitude to a peak amplitude and back to zero again. The time history is an odd function about the peak ramp amplitude so that the overall static input to the component is minimized. Peak amplitudes are determined by the load range of the desired component model.

After component test data is collected, an identification algorithm is implemented that fits postulated constitutive models to the data. Two algorithms are used, one for load-control[7] and the other for strokes-control[8] testing.

The algorithm for load-control test data is to separate the weak coupled loads (other than the dominant load) from a single load direction test and drive the current component model with them. The component model is integrated to give the residual states resulting from the weak coupled loads. These states are then used to correct the measured states so that the strong applied load direction data can be fit to the model (as a function of the multiple corrected DOF). The basis of the load-control identification algorithm is the following. To fit the strong load direction model, the measured states need to be corrected for the state contributions due to the measured weak coupled loads; in order to generate the state corrections, a component model is needed.

Stroke-control test data motivated a second type of identification algorithm. Here loads data are corrected with residual loads generated by evaluating the current component model using the measured states (other than dominant) in each test. In this algorithm the corrected loads present in each of the six direction tests are fit to the dominant single-DOF response of each test, in an iterative fashion (as multiple functions of the single dominant DOF). The basis of the stroke-control algorithm is the following. To fit the dominant single-DOF models to the loads, the measured loads need be corrected for the load contributions due to the measured nondominant states; in order to generate the loads corrections, a component model is needed.

Within both the load- and stroke-control identification algorithms, linear and nonlinear least squares algorithms are used to fit the models to the data. Scaled and weighted linear least squares[8] is used to fit analytic models, whereas the Levenberg–Marquart algorithm is used to fit nonanalytic models.

Component models resulting from the identification procedure are subsequently reduced and incorporated into a global structural models. This methodology is now applied to the MODE structural components.

MODE Component Hardware

The MODE hardware, tested as single components, consists of an erectable bay, an adjustable pretension deployable bay, and an alpha joint bay.

An erectable bay assembly is used in the MODE baseline configuration (Fig. 1) to mate the two four-bay deployable elements. The erectable component hardware consists of struts, standoffs, and nodes. The struts make up the diagonal, batten, and longeron trusswork. The bulk of a strut is series 500 Lexan epoxied into an aluminum sleeved lug. The lug fits into a cutout receptacle in the standoff unit. The standoffs are premounted to the aluminum nodes before receiving the struts. Once in place, the internally threaded sleeve is screwed tight, pressing against the fixed standoff, thus fixing the strut to a node.

One of the two deployable elements of the MODE STA incorporates an adjustable pretension bay. In this bay three possible pretension settings of the bracing wires are possible. The highest of these pretensions is equal to the pretensions of the remainder of the deployable element bays. Like all deployable structures, the STA deployable elements are potentially nonlinear. In addition to the pretensioned diagonal bracing wires, the bay contains four series 500 Lexan longerons with 6061 anodized aluminum locking knee joints. During deployment, the two sections of the longeron fold at the knee joint, and pivot about a graphite pin at each of the two cross section frame attachments. A more detailed description can be found in Refs. 6 and 7.

In the MODE alpha configuration (Fig. 1), the alpha joint bay replaces the erectable bay joining the two deployable elements. Longitudinal axial rotation is permitted by the alpha joint about an axle centered at the two interfacing aluminum plates. A stainless-steel 0.22-in.-diam ball bearing race with an outer radius of 2.75 in. allows rotation about the axle when in its operational configuration. The bearing interface mechanism is approximately 6.0 in. diam. At 45-deg intervals around the central mechanism, trios of Lexan rods are mounted, the ends of which converge to an aluminum plate. On the outermost surface of these aluminum plates, a screw sleeve and lug assembly is fixed for attachment to a standoff, which in turn can be connected to a bay node. In this fashion the axial rotation mechanism of the alpha joint is interfaced to the deployable truss elements in the MODE alpha configuration.

A cam at the center of the rotation mechanism is used to vary the axial preload in the component. Two preloads were possible, denoted high and low, depending on the position of the cam. The cam applies axial preload to a rotary friction pad, which resists rotation around the axis.

Component Data

MODE component data are now presented for the torsional DOF of the deployable, erectable, and alpha joint bays. Only the torsional DOF data are shown as they are pertinent to the component models desired for the global structure analysis. First, data are presented in a force-state map and in a load-stroke form where appropriate. For the data shown the transmitted force is referred to as M_z and the torsion DOF is referred to as θ_z, where the subscript z is the axial axis of each component. All data presented were sampled at 200 Hz over a test time of 10.235 s.

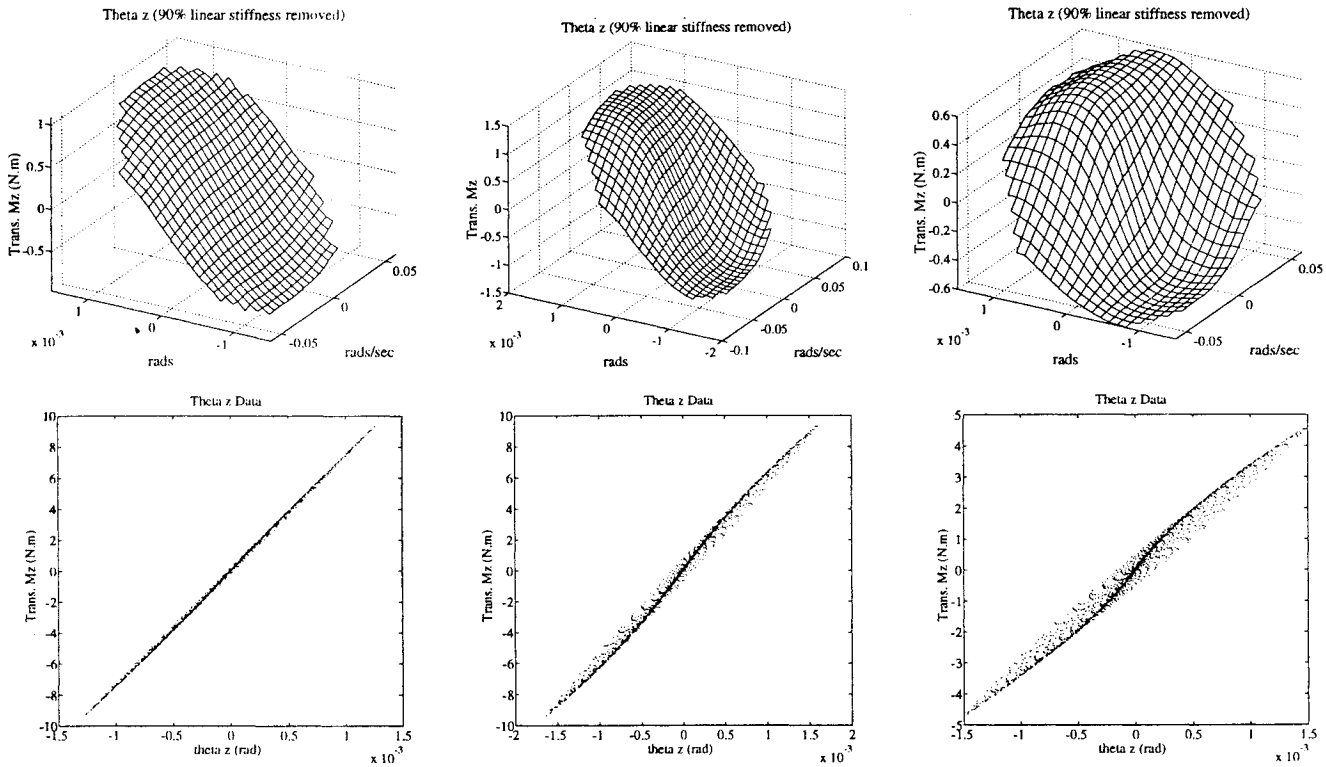

Fig. 2 Adjustable pretension bay force-state maps and load stroke plots for high (left), medium (center), and low (right) pretensions for commanded θ_z.

Data on the erectable bay are essentially linear and lightly damped and are omitted here for brevity.[8,9]

Adjustable pretension deployable bay tests were performed at 7.6 Hz for high, medium, and low wire pretensions and with stroke-control applied loads. Figure 2 shows the data in force-state map form for all three pretensions with 90% of the fit linear stiffness removed. The curvature in these maps clearly shows that dynamic hysteresis (nonlinear memory) is present in the data and that the severity of the dynamic hysteresis increases with decreased pretension in the bracing wires. In all three cases, the effect of the dynamic hysteresis is to soften and increase dissipation in the component with increased amplitude. The load-stroke plots confirm the magnitude of the nonlinearity increases with respect to the linear stiffness and that the linear stiffness decreases with decrease in pretension.

Within the load-stroke plots of Fig. 2 it can be seen that at lower amplitudes and higher pretensions the bay displaces as if the deployable pin joints were locked (by bracing wire preload). Here the bay is relatively linear and lightly damped. At higher amplitudes and lower pretensions the preloaded joints break into slip, physically softening and increasing the damping of the system. Further insights into this mechanism have previously been reported by the authors.[7,8]

Alpha joint bay tests were performed at the two possible mechanical preloads on the joint rotation axis, at 5-Hz test frequency and with load-control applied loads. For each preload, the data are presented in two regimes of alpha joint operation. The first regime is low amplitudes, where the motion is linear elastic-microfrictional in nature. In the second regime, at high amplitude, the friction pad mechanism is fully slipping and the motion exhibits classic coulomb frictional behavior.

Low-amplitude data show remarkable similarities between the adjustable pretension deployable bay (Fig. 2) and alpha joint bay hysteretic behavior (Fig. 3). The high-preload alpha joint bay data of Fig. 3 show softening and dampening with increased amplitude, as was the case with the adjustable pretension bay. The dynamic hysteresis in this data is due to the bearing race and friction pad microfrictional slippage.

High-amplitude load-stroke data for the high-preload alpha joint is plotted in Fig. 4. The data clearly show increased dissipation as strongly nonlinear boxlike hysteresis loops. In this type of hysteresis

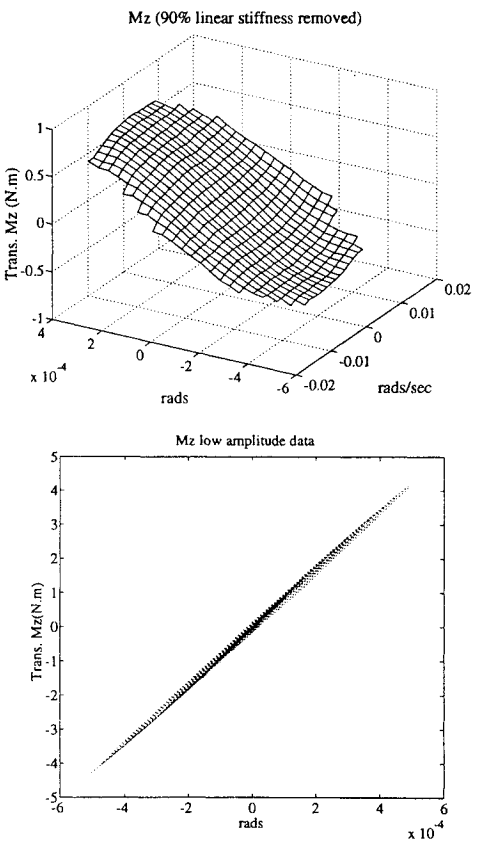

Fig. 3 MODE alpha joint high-preload, low-amplitude force-state map, and load-stroke plot for commanded M_z.

loop, the stiffness decreases and dissipation increases approximately linearly with amplitude. Displacement dependent friction is seen at the extrema of the transmitted load (regions 1, 3, 4, and 6) and low-amplitude microfriction is seen in regions 2 and 5. The behavior is qualitatively similar for the low preload, where the break load decreases significantly to approximately 30% of the high preload value.[9]

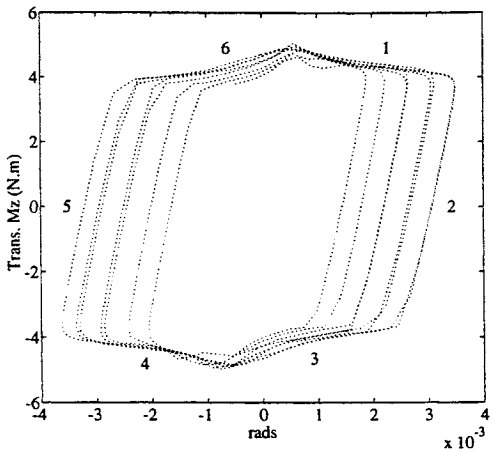

Fig. 4 MODE alpha joint high-preload, high-amplitude data for commanded M_z.

Reduced Component Models

Reduced models of the MODE component were obtained and subsequently used in the baseline and alpha configuration global models. The reduction was a three step process. First, physically derived 12-DOF beam element component models were derived from the multiple DOF data,[7,8] the torsion DOF of which was shown in Fig. 2. Second, these models were reduced to models of the global axial moment/torsion DOF only. Finally these single-DOF models were approximated by analytic polynomial models. The analytic polynomial models are presented here before presenting their correlation to the data.

Both the adjustable pretension deployable bay and alpha joint bays exhibit dynamic hysteresis in their torsional response. This is due to the microfriction generated in the preloaded pin joints of the adjustable bay and in the friction pad and bearing race of the alpha joint bay. Physically derived models of these components showed that nonlinear memory is inherent in microfrictional systems.[7,8] The conditional nonlinear memory models of the adjustable pretension and alpha joint bays are cumbersome to compute in global structure dynamics analysis. The physical models are, therefore, approximated with analytical polynomial functions in the appropriate dynamic range.

A bicubic polynomial function is used for the adjustable pretension deployable bay

$$F_{D_{h,m,l}} = \sum_{m=0}^{3}\sum_{n=0}^{3} C_{mn}\theta^m\dot{\theta}^n \tag{1}$$

where $F_{D_{h,m,l}}$ is the transmitted moment resulting from the torsion motion of the deployable D bay for each of high h, medium m, and low l preload. Note that the bicubic analytic model includes products of rotation and rotation rate states, providing a mechanism for stiffness and dissipation coupling.

Two biquartic polynomial functions are used for each preload, high h and low l, in the alpha joint A bay

$$F_{A_{h,l}} = \begin{cases} \sum_{m=0}^{4}\sum_{n=0}^{4} C_{mn}\theta^m\dot{\theta}^n & 0 < \theta < \delta_{br} \\ \sum_{m=0}^{4}\sum_{n=0}^{4} C'_{mn}\theta^m\dot{\theta}^n & \delta_{br} < \theta < 4\delta_{br} \end{cases} \tag{2}$$

Transmitted moment across the alpha joint, $F_{A_{h,l}}$, is approximated in two separate ranges by biquartic functions. The first biquartic function models the microfriction range $0 < \theta < \delta_{br}$, where δ_{br} is the amplitude at which the friction pad mechanism breaks into fully engaged slip. The second biquartic function models the macrofriction range $\delta_{br} < \theta < 4\delta_{br}$.

In contrast to the adjustable pretension and alpha joint bays, the erectable bay component is predominantly linear with joints tightly fastened.[8] It is sufficient to model the erectable hardware torsion DOF with a linear stiffness term and a linear dissipation term

$$F_E = C_{10}\theta + C_{01}\dot{\theta} \tag{3}$$

where the linear coupling between the axial and torsion DOF within the component has been ignored in the transmitted moment F_E.

The correlated coefficients of the reduced analytic models [Eqs. (1–3)] to the component data presented are listed in Table 1 of Ref. 9. For the alpha joint models, the low-amplitude biquartic models were fit to the amplitude range $[0, 1.2\delta_{br}]$ and the high-amplitude biquartic models were fit to the range $[0.8\delta_{br}, 4\delta_{br}]$. Overlapping the state range over which the models were fit allows a transition within each alpha joint model (high and low preload). The transition is mildly discontinuous in transmitted force. The discontinuity is reduced by fitting the biquartic functions to an intersecting range.

Global Structure Modeling and Refinement

Now that the multiple DOF force-state component identification methodology has been applied to the MODE components, the results are used in global structure modeling. The reduced component models of the adjustable pretension deployable bay, erectable bay, and alpha joint bay are assembled to model the torsion DOF of the baseline and alpha MODE configurations. This section describes how the component models are assembled, first of the baseline and then the alpha configurations. Some model refinement is then performed.

Global Configuration Models

The assembled model of the baseline structure uses the adjustable pretension bay models, F_D, and erectable bay model, F_E, as shown in Fig. 5. All deployable bays use the high-preload model, F_{D_h}, except for the third from the left, which was appropriately selected to represent high-, medium-, or low-pretension baseline models. Suspension springs that grounded the model were linear and mimicked the (1-Hz plunge mode) ground dynamics test suspension springs. For the space test analyses, these springs were arbitrarily reduced by more than an order of magnitude to simulate free end conditions.

The inertias used (Fig. 5) lump that of the components and the MODE structure end masses. The end inertias I_1 and I_{10} dominate the inertia matrix. Actuator inertia is added to I_1 to model the added inertia from proof mass actuator that forces the structure.[9]

In the alpha configuration model, the alpha joint component models replace the erectable component model as the center spring as shown in Fig. 5, where F_{A_h} incorporates both low- and high-amplitude models of the joint as does F_{A_l}. In the MODE alpha configuration all of the deployable nonlinear springs are represented by F_{D_h} corresponding to the adjustable bay in high pretension.

Even though the MODE physical structure (infinite DOF) and the MODE models (10 DOF) are fundamentally different, the dynamic results near the torsion mode should be fairly accurate. This assumption is based on the fact that near the fundamental mode of the structure, the torsion DOF dominate the structural response.

Third-Generation Model Refinement

The component models $F_{D_{h,m,l}}$ and $F_{A_{h,l}}$ are further refined in order to produce dynamic predictions more consistent with the low-amplitude force input ground tests. Two types of refinement are performed. The first type of refinement is a third-generation model update that seeks to more accurately represent gravity loading of the structure suspended in the laboratory. This refinement is needed as the component models are based on the unpreloaded component data. The second type of refinement is a third generation model update to the linear stiffness terms of the adjustable pretension and alpha component models. These are refined to better match the low-amplitude force ground test resonant frequencies.

Gravity loads were present in the MODE baseline and alpha ground dynamics tests. The gravity loads were generated in part by the offset of the end mass center of gravity from the suspension connect points. The static gravity loads in the structure preloaded the pin joints of the deployables and the friction pad of the alpha joint over and above the internal component preloads present in the component testing.

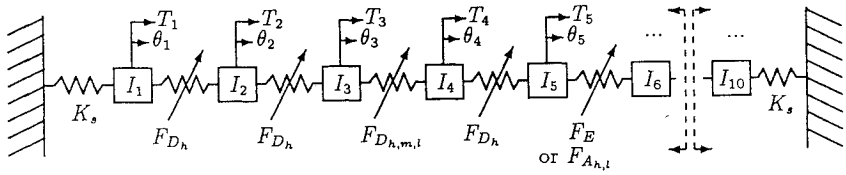

Fig. 5 MODE STA 10-DOF model torsion axis, baseline, and alpha configurations.

For the analyses, of ground testing only, the nonlinear terms in the component models [the C_{mn} of Eqs. (1) and (2), where $mn \neq 01, 10$] are multiplied by a participation factor of 0.6. Reducing the participation of the nonlinear parameters is equivalent to further preloading the sliding and rotational interfaces of the components. This simulates a gravity preload on the structure.

Refinement of the linear stiffness terms in the adjustable pretension bay and alpha joint bay component models is performed and maintained for both ground and space analyses. The refinements result from comparing linear eigenanalysis of the 10-DOF MODE assembled component models and the measured frequencies of the low input force ground dynamics data. The linear stiffness terms C_{10} in Eq. (1) of the adjustable pretension bay models $F_{D_{h,m}}$ are multiplied by a factor of 0.9, and the C_{10} of F_{D_l} is multiplied by a factor of 1.3. These adjustments reflect a measured trend in the ratio of the static bracing wire pretensions between the MODE deployable structure, used in modal testing, and the adjustable pretension deployable component, used in the force-state tests. Measured pretensions in the four-bay deployable section of the MODE structure were approximately 7, 13, and 27 lbs for low, medium, and high pretensions, respectively. The adjustable pretension bay used in component testing measured pretensions were approximately 4, 15, and 32 lbs, respectively. The low pretension of the test component was, therefore, too low (motivating the multiplication by 1.3), whereas the medium and high pretensions were too high, motivating a factor of 0.9.

The linear stiffness terms in the high- and low-preload alpha joint models $F_{A_{h,l}}$ were also multiplied by 0.9 based on low-force ground dynamics data. A possible justification for this update is slightly differing break loads in the MODE alpha joint used in modal testing and the alpha joint test component.

Global Analysis Method

Computing the response of nonlinear dynamics models of the MODE baseline and alpha configurations was a difficult task. The difficulty arose from the low damping present in the 10-DOF MODE models combined with the low to moderate nonlinearity of the components. In this section, an algorithm for computing the global response of the MODE models is presented.

To make a direct comparison between the MODE models and the data, a computational method was derived that computes the output harmonic amplitude resulting from excitation at a specific frequencies and amplitude. The method was derived from a combination of existing methods and entitled direct linearization analysis (DLA).

In this section DLA is presented as a combination of the alternating frequency-time domain method[10] and the single-frequency harmonic balance (HB) methods.[11] The objective of DLA is to step through a discrete frequency window, computing the linearized (M, C, K) and complex harmonic response at each frequency point for a specific excitation amplitude.

DLA iterates on the linear stiffness and damping matrices that fit the response of the model in a least squares sense at each frequency point (the inertia matrix is assumed constant). The underlying concept is that convergence of the fit stiffness and damping matrices means convergence of the linearized harmonic response at a discrete frequency of input. The method relies on the existence of an average linear model.

Figure 6 shows the flow of the DLA algorithm that was applied to the MODE baseline and alpha models. The logic outlined in Fig. 6 proceeds as follows.

Step 1: The linear stiffness and damping matrices K_L and C_L are formulated from component models evaluated at low amplitudes. M_L is constant for the MODE models.

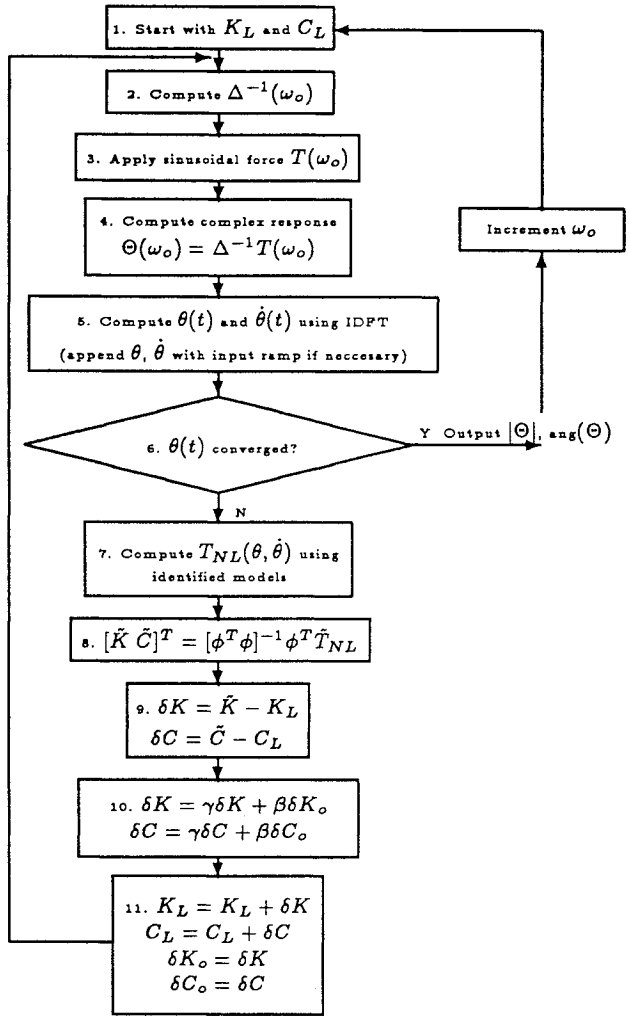

Fig. 6 Flow for direct linearization analysis.

Step 2: The system matrices M_L, C_L, and K_L are used to compute the frequency-domain structural operator $\Delta(\omega)^{-1}$ at the input force frequency ω_0 according to

$$\Delta^{-1} = \left(-\omega^2 M_L + j\omega C_L + K_L\right)^{-1} \tag{4}$$

Step 3: The frequency-domain vector of applied (co)sinusoidal torques $\boldsymbol{T}(\omega)$ is generated.

Step 4: The complex linear response $\boldsymbol{\Theta}$ at the input frequency ω_0 is computed by inverting the complex structural operator and premultiplying it to the vector of applied torques $\boldsymbol{T}$.

Step 5: The complex response $\boldsymbol{\Theta}$ is used to generate the time domain-response $\boldsymbol{\theta}(t)$ and $\dot{\boldsymbol{\theta}}(t)$. If necessary, ramped sinusoids are appended to the beginning of the constant amplitude sinusoids for modeled memory computations. For the MODE models this is not necessary due to the analytic nature of the approximate component models.

Step 6: Convergence of the time-domain response is tested. For the MODE models, a relative error check was used. The relative error is defined as

$$\theta_{\text{err}} = \int |\theta_i(t) - \theta_{i-1}(t)|\,dt \Big/ \int \theta_{i-1}^2(t)\,dt \tag{5}$$

The tolerance used for the MODE models was 1%.

Step 7: If convergence is not achieved, the matrix of quasistatic component torques $T_{NL}(\theta, \dot{\theta})$ is computed using the current nonlinear structural model. The kth column of T_{NL} is the quasistatic force generated in the kth bay of the structural model.

Step 8: Linear parameters are least squares fit, arranged as the appropriate vector $[\tilde{K}\ \tilde{C}]^T$ to the matrix of torques, arranged as the appropriate vector $\tilde{T}_{NL}$. Equation (6) shows how the simulated data matrix ϕ of relative rotations and rotation rates is formulated,

$$\phi = [(\theta_2 - \theta_1) \quad (\theta_3 - \theta_2) \cdots (\dot{\theta}_2 - \dot{\theta}_1) \cdots] \tag{6}$$

Block 8 in Fig. 6 shows the least squares fit equation.

Step 9: The perturbation stiffness and damping matrices δK and δC are obtained by subtracting off the previous linear part.

Step 10: This step relaxes δK and δC with the last iteration solution providing some smoothing to the procedure. For the MODE computations, $\gamma = \frac{2}{5}$ and $\beta = \frac{3}{5}$ were used. Terms previous to the last solution can be used at the expense of memory storage.

Step 11: The new linear stiffness and damping matrix pair K_L and C_L are found. The results of the iteration are stored before restarting at step 2.

The converged output is the complex amplitude and angle of the response. After convergence is achieved, the complex response is stored and the driving frequency is incremented. The solutions from the last frequency step, K_L and C_L, are now used as an initial guess for the new driving frequency.

Predictions and MODE Modal Data

The results of applying the DLA to the assembled MODE global models are compared to the test data. As a preface, the presented modal data and the inputs and outputs of the DLA of the MODE models are specified. The results of DLA of the MODE baseline and alpha models are compared to ground and space modal test data in terms of discrete frequency-domain response, fit natural frequencies, and fit damping ratios.

Selected dynamics modal test data are given in this section for comparative purposes. These data, shown in Figs. 7–10, are presented as pointwise frequency-domain ratios of the output harmonic amplitude (units of gravity, g) to the input harmonic amplitude (units of force, pounds force). These discrete frequency domain curves were circle fit by Crawley et al.[6] to give natural frequencies end damping ratios.

The torques that were used to drive the baseline and alpha MODE models are derived from measurements made during the MODE dynamics tests.[6] Input torques drive the model at I_1 (see Fig. 5), which is consistent with the proof mass actuator (PMA) location at one end of the MODE truss.[6]

Predictions from the DLA are shown in this section as the harmonic ratio of the acceleration $\ddot{\theta}_1$, in units of gravity, to input PMA force, in pounds force. The predictions are plotted in the discrete frequency domain on frequency and magnitude scales equivalent to the presented MODE data. The predictions were circle fit with the same routine as the MODE data and tabulated values of natural frequency and damping ratio are compared.

Baseline Configuration

Figures 7 and 8 show the MODE baseline data for both space and ground (top) vs DLA predictions (bottom) for high and low pretensions in the adjustable bay, respectively.

In general, the predicted ground magnitudes compare well to that of the data. In both the space predictions and data, the magnitudes are less than the ground magnitudes. This is, to a lesser degree, due to the increased damping. The majority of the decreases in magnitude between space and ground is caused by the removal of the suspension system. The space predictions clearly do not decrease in magnitude as severely as the space data. The space data, however, also include residues from actuator dynamics.

The predictions, shown in Figs. 7 and 8, clearly capture nonlinear dynamic hysteresis in the discrete frequency domain. The predictions show a softening and dampening torsional mode as the input force level is increased. By comparing the high-pretension predictions of Fig. 7 with the low-pretension predictions of Fig. 8, it is seen

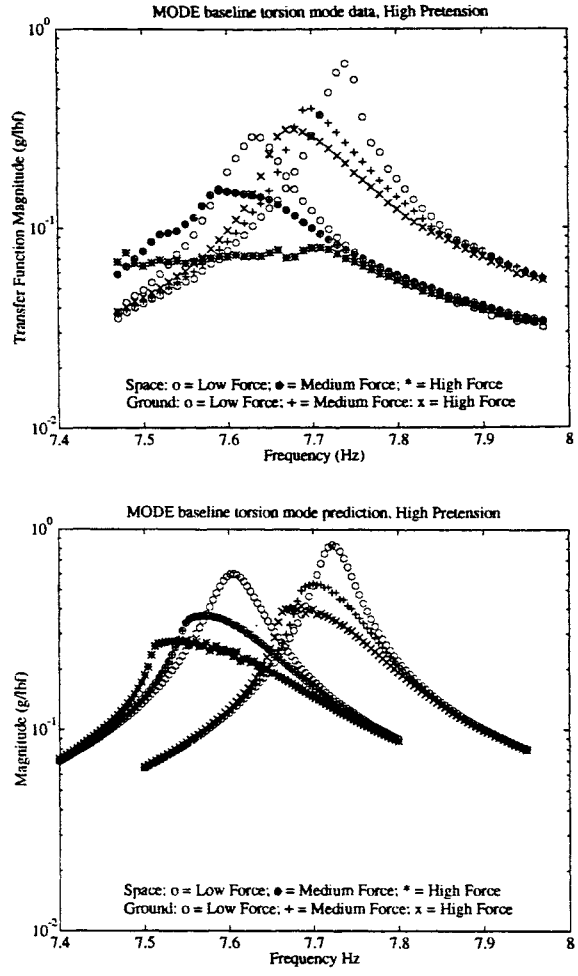

Fig. 7 Ground vs space comparison of modal data and predicted response, MODE baseline, high pretension.

that this nonlinear behavior increases in severity with decrease in wire pretension. These predicted results are consistent with the data.

Space predictions show softening and dampening that is, in part, consistent with the space data. Some other phenomena present in the space data are not predicted by the DLA. The increased dissipation in the space data may be due to erectable joint loosening, although joint loosening does not occur without softening of the erectable component (as shown by the authors[8]), which is not clearly evident in the data. Another guise of apparent increased harmonic dissipation is randomly transitional behavior, or chaos.[12]

Low-input forces result in the most linear and lightly dampened fundamental mode predictions. This is consistent with the MODE dynamics data shown and also with the low-amplitude component data.

Low-level apparent noise in the predicted response plots was due to convergence problems in the DLA. The linearized matrices K and C tended to two distinct but slightly varying solutions. This solution bifurcation may be the result of multiple solutions or the fact that the direct method incorporated weak numerical limit cycles.

Table 1 lists the comparison of the circle fit natural frequencies and damping ratios of the ground baseline data and model predictions. The fit modal parameters show agreement in frequency of 0.5% and in damping of 0.1% (good by any measure of damping at this level). When comparing the ground predictions to the data, it must be reiterated that a third generation update was performed to adjust the linear stiffness C_{10} based on the ground low-force resonant frequency data. Given that the update was performed, the nonlinear MODE model correctly predicts the frequency trends for increased input force and correctly predicts the damping ratios and trends.

Table 1 also lists the comparison of the circle fit natural frequencies and damping ratios of the space data and model predictions for the baseline configuration. Space predictions were made after

Table 1 Ground test vs predicted natural frequencies and damping ratios, MODE baseline configuration

	Modal parameters			
	Modal data fit		Prediction	
Amplitude	ω, Hz	ζ, %	ω, Hz	ζ, %
Ground:				
Hi pr: low	7.74	0.24	7.72	0.26
med.	7.70	0.40	7.70	0.44
high	7.67	0.54	7.68	0.57
Me pr: low	7.71	0.27	7.68	0.34
med.	7.66	0.42	7.66	0.49
high	7.64	0.57	7.63	0.62
Low pr: med.	7.58	0.67	7.59	0.60
high	7.54	0.86	7.55	0.74
Space:				
Hi pr: low	7.63	0.40	7.60	0.36
med.	7.59	0.92	7.57	0.62
high	7.57	no fit	7.54	0.81
Me pr: low	7.61	0.34	7.56	0.50
med.	7.57	no fit	7.52	0.71
high	7.53	no fit	7.48	0.89
Low pr: med.	7.52	no fit	7.47	1.01
high	7.49	no fit	7.42	1.19

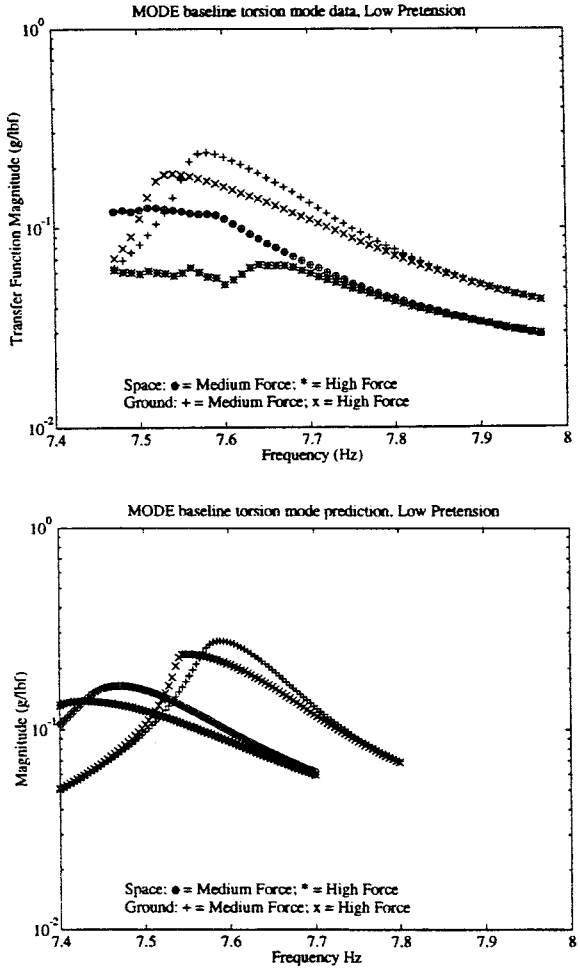

Fig. 8 Ground vs space comparison of modal data and predicted response, MODE baseline, low pretension.

removal of suspension and gravity effects in the model. The modal parameters in Table 1 show good agreement in frequency of approximately 0.5% and general disagreement in damping. This shows that the model correctly predicts the stiffness effects of the change in gravity environment. Although the trend in damping predictions is correct, the disagreement in quantitative damping is obvious in Figs. 7 and 8, where it can be seen that the space data exhibit flattened magnitude behavior. The tabulated space predictions show increased

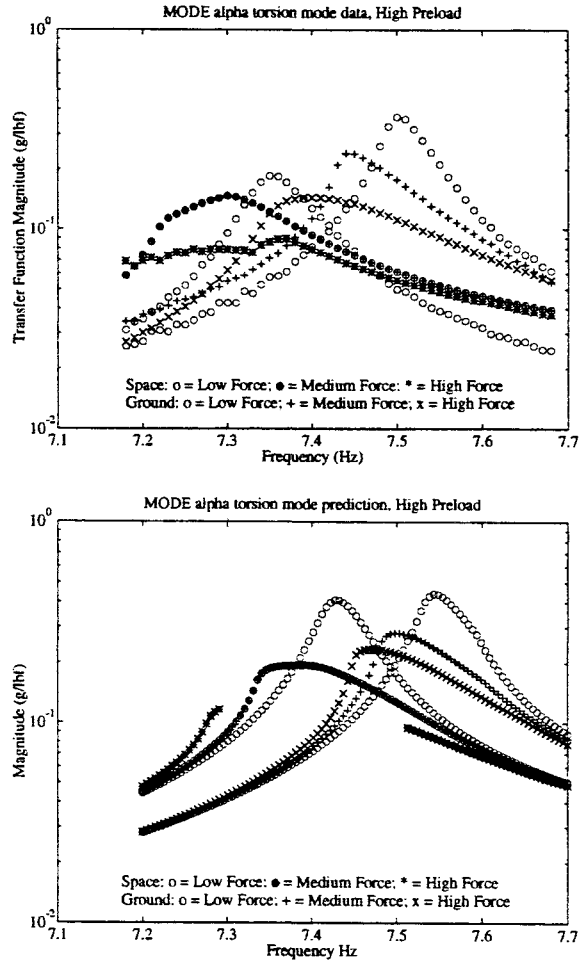

Fig. 9 Ground vs space comparison of data and predicted response, MODE alpha configuration, high preload.

damping with increased input force level but not of the same order as the data.

Alpha Configuration

Selected results of the MODE alpha predictions are shown in Figs. 9 for high-alpha preload and Figs. 10 for low-alpha preload. In the MODE alpha model, the nonlinear behavior of the adjustable pretension deployable bays (all in high pretension) is compounded with that of the alpha joint bay nonlinearity.

Figure 9 shows the ground and space data and predictions for the high-preload MODE alpha configuration. First, note the change in resonant frequency after the inclusion of the alpha joint. This can be seen by comparing Figs. 7 and 9, keeping in mind that a third generation update has been performed on the linear stiffness of both the baseline and the alpha model. Further comparison of Figs. 7 and 9 shows that the softening and dampening of the torsion mode with increased input amplitude are of greater severity in the alpha data and predictions. The ground data and predictions show that microslippage dynamic hysteresis that is present in the alpha joint bay at amplitudes below the break amplitude serves to further soften and dampen the response over that of the baseline.

Again the space magnitude data presented tends to severely dampen and flatten out with increased input force. The predicted space results show similar softening and dampening with increased input force level but, again, with not as great a change as the data. The space high-force predictions did not converge to a solution in the frequency range 7.3–7.5 Hz. This region is where the alpha joint breaks into full slipping of the rotary mechanism. The solutions of the DLA in this region were seen to vary without converging. Full slipping motion in the alpha joint results in a drastic change in the structure. The high-preload space data show a substantial region, below 7.37 Hz, where the magnitude of the response has been severely reduced. This indicates that the alpha joint mechanism is slipping.

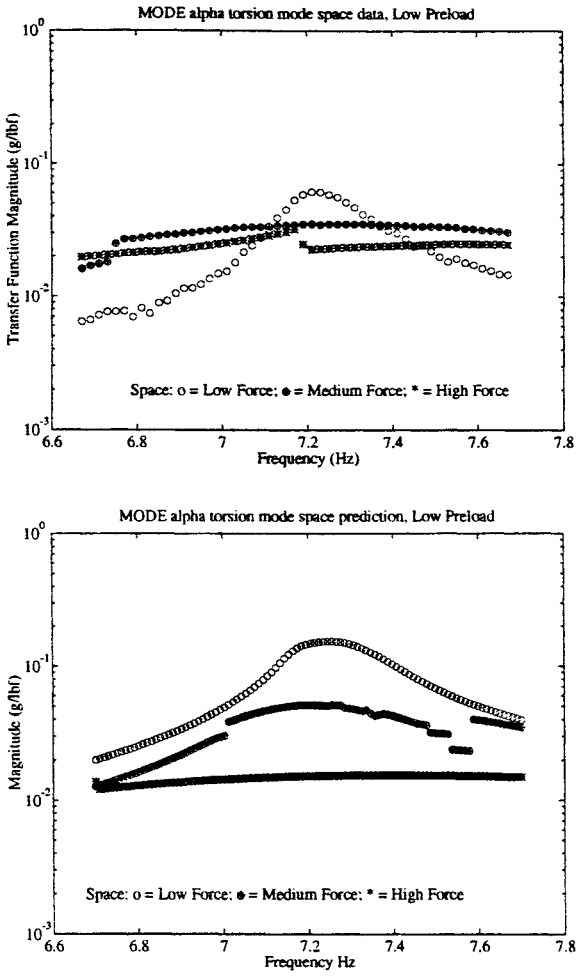

Fig. 10 Comparison of space data and predicted response, MODE alpha configuration, low preload.

Figure 10 shows the low-preload MODE alpha data and prediction for space only. Mechanism slipping behavior is witnessed in both the data and in the predictions as moderately nonlinear jump behavior. The predictions show jumps similar to that occurring in the space data. Jumps are predicted at medium- and high-forcing levels. The medium-force predicted response shows multiple jumps in the region where the alpha joint mechanism is engaged, 7.03–7.56 Hz. For the high-input force, the MODE alpha predictions show the alpha joint to break into mechanism slippage at around 6.7 Hz and not recover microslippage behavior within the frequency window. This shows remarkable similarity to the high-input force data.

The effect of the alpha joint mechanism slipping is to separate the deployable structural sections with a spring and dashpot that both soften and dampen linearly with increased response amplitude. The alpha joint transmits loads to the remainder of the structure while the mechanism is slipping. The drastic drop in stiffness and increase in damping with response amplitude, however, serve to flatten out the fundamental mode.

Predicted modal parameters are compared to the modal parameters fit to the data in Table 2. For the comparison of the ground modal parameters, it is again reiterated that an update of the linear stiffness of the alpha joint models was made based on the low-force ground data natural frequencies. The parameters show that the predicted ground natural frequencies are good to within 1% where appropriate. Increased damping with increased input amplitude is predicted within 0.45% for the high-preload ground results. This shows that the compounded dynamic hysteresis mechanisms of the deployables and the alpha joint provide further softening and dampening, with increased input force level, over that witnessed in the baseline data and predictions.

Space results reported in Table 2 show the frequencies are predicted within 1.5%, whereas the increase in damping is predicted within 0.25% for the shown modal parameter fits. As with the baseline results, the change in environment has been adequately predicted by the model.

Table 2 Modal test vs predicted natural frequencies and damping ratios, MODE alpha configuration

	Modal parameters			
	Modal data fit		Prediction	
Amplitude	ω, Hz	ζ, %	ω, Hz	ζ, %
Ground:				
Hi pr: low	7.50	0.37	7.54	0.39
med.	7.44	0.53	7.49	0.60
high	7.39	1.13	7.46	0.72
Low pr: low	7.41	1.37	7.45	1.01
med.	7.16	2.50	7.35	>10
high	no fit	no fit	no fit	no fit
Space:				
Hi pr: low	7.35	0.51	7.43	0.41
med.	7.30	1.07	7.37	0.95
high	7.24	no fit	no fit	no fit
Low pr: low	7.21	1.21	7.32	0.98

Conclusions

A force-state component identification methodology was presented. The features of the methodology include a unique 6-DOF testing device for testing structural components and load- and stroke-control identification algorithms. The methodology was applied to typical deployable, erectable, and rotary joint structural components.

Data on the deployable and alpha joint structures showed fundamental dynamic hysteresis behavior as a result of microfrictional response under load excitation. Decrease in deployable pretension and decrease in alpha joint preload increased the severity of the dynamic hysteresis. At rotation amplitudes above the break amplitude, the alpha joint rotation mechanism was seen to be fully engaged, exhibiting coulomb like softening and dampening with increasing rotation amplitude.

Updated analytic polynomial models that coupled rotation and rotation rate states were used to describe the nonlinear component data, and, in turn, were assembled to investigate the torsion mode of typical baseline truss and alpha joint structures. A DLA algorithm was developed that stepped discretely in excitation frequency and computed the (successively linearized) nonlinear response of the models for multiple levels of excitation.

Predictions from the analysis algorithm compared well with the data, confirming that the component nonlinear mechanisms, acting quasistatically, are major contributors to the overall nonlinear structural response. Further nonlinear effects present in the space data appeared to have severely dampened the fundamental mode at high levels of excitation and are apparently not due to the quasistatic nonlinear nature of the components. Fit modal parameters predicted changes in frequency and damping of the fundamental torsion mode with increased amplitude of excitation and change in gravity environment. Analysis of the alpha joint model also predicted nonlinear jump phenomena in the discrete frequency response, consistent with that witnessed in data.

Acknowledgments

This work was supported by NASA Instep Flight Experiments Program and NASA Langley Research Center Reference NAS1-18690, with Sherwin Beck as monitor, and by NASA Headquarters Grant NAGW-1335 to the MIT Space Engineering Research Center, with Robert Hayduk as technical monitor.

References

[1]Balmes, E., "A Finite Element Updating Procedure Using Frequency Response Functions. Applications to the MIT/SERC Interferometer Testbed," International Modal Analysis Conference (Honolulu, HI), 1993, pp. 176–182.

[2]Nayfeh, A. H., Mook, D. T., and Lobitz, D. W., "Numerical-Perturbation Method for the Nonlinear Analysis of Structural Vibrations," *AIAA Journal*, Vol. 12, No. 9, 1974, pp. 1222–1228.

[3]Woinowsky-Krieger, S., "The Effect of an Axial Force on Vibrating Hinged Bars," *Journal of Applied Mechanics*, Vol. 17, No. 1, 1950, pp. 35–37.

[4]Belvin, W. K., "Modeling of Joints for the Dynamic Analysis of Truss Structures." NASA Langley Research Center Rept. NASA-TP-2661, May 1987.

[5]Chapman, J. M., Shaw, F. H., and Russell, W. C., "Nonlinear Transient Analysis of Joint Dominated Structures," AIAA Paper 87-0892, April 1987.

[6]Crawley, E. F., Barlow, M. S., van Schoor, M. C., Masters, B. P., and Bicos, A. S., "Middeck Zero-Gravity Dynamics Experiment: Comparison of Ground and Flight Test Data," 43rd Congress of International Astronautical Federation, Washington, DC, Aug.–Sept. 1992; *Journal of Guidance, Control, and Dynamics* (to be published).

[7]Masters, B. P., and Crawley, E. F., "Multiple Degree of Freedom Force-State Component Identification," *AIAA Journal*, Vol. 32, No. 11, 1994, pp. 2276–2285.

[8]Masters, B. P., and Crawley, E. F., "Multiple Degree of Freedom Force-State Component Identification," Dept. of Aeronautics and Astronautics, Space Engineering Research Center, Rept. 1-94, Massachusetts Inst. of Technology, Cambridge, MA, Jan. 1994.

[9]Masters, B. P., Crawley, E. F., and van Schoor, M. C., "Global Structure Modeling Using Force-State Component Identification," AIAA Paper 94-1519, April 1994.

[10]Cameron, T. M., and Griffin, J. H., "An Alternating Frequency/Time Domain Method for Calculating the Steady-State Response of Nonlinear Dynamic Systems," *Journal of Applied Dynamics*, Vol. 56, March 1989, pp. 149–154.

[11]Gelb, A., and Vander Velde, W. E., *Multiple-Input Describing Functions and Nonlinear System Design*, McGraw–Hill, New York, 1968, Chaps. 2–4.

[12]Ueda, Y., "Randomly Transitional Phenomena in the Systems Governed by Duffings Equation," *Journal of Statistical Physics*, Vol. 20, No. 2, 1979, pp. 181–196.